

Supporting Information

Wide Bandgaps and Strong SHG Responses of Hetero-Oxyfluorides by Dual-Fluorination-Directed Bandgap Engineering

Yilei Hu,^{+a} Xingxing Jiang,^{+b} Tianhui Wu,^{+a} Yanyan Xue,^{+a} Chao Wu,^{*a} Zhipeng Huang,^a
Zheshuai Lin,^b Jun Xu,^a Mark G. Humphrey,^c and Chi Zhang^{*a}

^a China-Australia Joint Research Center for Functional Molecular Materials, School of Chemical
Science and Engineering, Tongji University, Shanghai 200092, China

^b Technical Institute of Physics and Chemistry, Chinese Academy of Sciences, Beijing 100190,
China

^c Research School of Chemistry, Australian National University, Canberra, ACT 2601, Australia

⁺ These authors contributed equally.

Table of Contents

| | |
|---|-------|
| Section S1. Materials and Methods..... | S3–S5 |
| Table S1. Crystallographic data and structure refinement parameters for RWOFI and CWOFI..... | S6 |
| Table S2. Selected bond distances (Å) and angles (deg) for RWOFI..... | S7 |
| Table S3. Selected bond distances (Å) and angles (deg) for CWOFI..... | S8 |
| Table S4. Atomic coordinates, equivalent isotropic displacement parameters, and bond valence sums for each atom in the asymmetric unit of RWOFI..... | S9 |
| Table S5. Atomic coordinates, equivalent isotropic displacement parameters, and bond valence sums for each atom in the asymmetric unit of CWOFI..... | S10 |
| Table S6. Calculated magnitudes and directions of dipole moments of RWOFI and CWOFI...S11 | |
| Table S7. Contributions of different groups to the SHG response and birefringence of RWOFI and CWOFI..... | S12 |
| Figure S1. Experimental and simulated powder X-ray diffraction patterns of RWOFI (a) and CWOFI (b)..... | S13 |
| Figure S2. Scanning electron microscope images and energy dispersive spectroscopy results of RWOFI (a) and CWOFI (b)..... | S14 |
| Figure S3. Out-of-center distortion for W ⁶⁺ in CWOFI; the distortion is away from the oxide ligands that link to a lone-pair cation..... | S15 |
| Figure S4. IR transmission spectra from single crystals (a, b) and crystalline powder samples (c, d) of RWOFI and CWOFI. The inserts show the detailed IR absorption peaks..... | S16 |
| Figure S5. Thermogravimetric analyses of RWOFI (a) and CWOFI (b) under a N ₂ atmosphere..... | S17 |
| Figure S6. Calculated band structures of RWOFI (a) and CWOFI (b)..... | S18 |
| Figure S7. Calculated density of states (a) and refractive indexes (b) in CWOFI. SHG-weighted density for (c) occupied and (d) unoccupied states in the virtual electron process for CWOFI. Color codes: I brown, Mo green, O red, F light green, Cs purple..... | S19 |
| References | S20 |

Section S1 Materials and Methods

1. Hydrothermal Syntheses

The starting materials Cs₂CO₃ (99.9%, Xiya), Rb₂CO₃ (99.9%, Xiya), H₅IO₆ (99.0%, Xiya), WO₃ (99.8%, Xiya), and HF (40%, Aladdin) were commercially purchased and used immediately without further purification. *Caution! Hydrofluoric acid is poisonous and corrosive. The highest care is essential and appropriate protection must be applied.*

The crystals of Rb₂WO₂F₃(IO₂F₂) (RWOFI) and Cs₂WO₂F₃(IO₂F₂) (CWOFI) were synthesized by a hydrothermal method. For RWOFI, 0.462 g (2.00 mmol) of Rb₂CO₃, 0.556 g (2.00 mmol) of H₅IO₆, 0.928 g (4.00 mmol) of WO₃, and 2.0 ml HF were used. For CWOFI, 0.652 g (2.00 mmol) of Cs₂CO₃, 1.112 g (4.00 mmol) of H₅IO₆, 0.464 g (2.00 mmol) of WO₃, and 2.0 ml HF were used. All reagents were added into 23 mL Teflon-lined autoclaves. These pouches were sealed and heated to 230 °C and held for 96 h, and then cooled to room temperature at a rate of 4 °C/h. After that time, colorless rod-like crystals of RWOFI and CWOFI were separated using a microscope. The yields of RWOFI and CWOFI were up to 90–95% (based on W).

2. Single-Crystal Structure Determination

High-quality transparent crystals were selected and cut into the proper size, mounted on a glass fiber, and inserted into the goniometer head for single-crystal structural determinations. A Bruker D8 VENTURE CMOS X-ray source was used to produce Mo K α radiation ($\lambda = 0.71073\text{\AA}$) at room temperature. Single-crystal X-ray diffraction data of RWOFI and CWOFI were obtained, integrated, and reduced by APEX II software with a multiscan-type model to obtain the absorption corrections. The crystal structures were solved and refined on F^2 by full-matrix least-squares methods using the *SHELXTL-2017* software.^[1] All non-hydrogen atoms were refined with anisotropic displacement parameters. The absolute structures were examined using PLATON and no omitted symmetry elements were found.^[2] The Flack factor of CWOFI was refined to be 0.02(2), indicating the correctness of its absolute structure. The Flack factor of RWOFI was 0.32(10), indicating that RWOFI is a racemic twin crystal. A summary of crystal data and structure refinement information is given in Table S1. Selected bond distances (Å) and angles (°) are

collected in Tables S2–S3. Atomic coordinates and equivalent isotropic displacement parameters are given in Tables S4–S5. The details of the crystal structures (CCDC-2164004 for RWOFI and CCDC-2164005 for CWOFI) can be obtained from the Cambridge Crystallographic Data Centre via www.ccdc.cam.ac.uk/data_request/cif.

3. Instruments and Methods

3.1 Powder X-ray Diffraction

The powder X-ray diffraction (PXRD) analysis was performed to confirm the purity of the crystalline sample (Figure S1). The patterns were recorded on a Bruker D8 ADVANCE X-ray diffractometer using monochromated Cu K α radiation ($\lambda = 1.5418 \text{ \AA}$), in the 2θ range 5 to 70°, with a step width of 0.02° and a scanning speed of 0.5 s/step at room temperature.

3.2 Energy-Dispersive X-ray Spectroscopy

Microprobe elemental analyses were measured using an energy-dispersive X-ray spectroscope (EDS) with a field-emission scanning electron microscope (Hitachi S-4800, Japan).

3.3 Optical Transmission Spectra

The optical transmission spectra in the UV-Vis-NIR (200–2500 nm) and IR (2.5–25 μm) regions were recorded on a Cary 5000 UV-Vis-NIR spectrophotometer and a Nicolet iS10 Fourier transform infrared (FTIR) spectrometer, respectively. Single crystals of $0.8 \times 0.4 \times 0.2$ and $1.8 \times 0.4 \times 0.4 \text{ mm}^3$ were used to perform the UV-Vis-NIR measurements. The IR spectra were measured over the wavenumber range 500–4000 cm^{-1} by the KBr powder-compression method. The samples were mixed thoroughly with dried KBr at a mass ratio of about 1:100 and were then pressed into transparent sheets for measurements.

3.4 Thermal Stability

A Netzsch STA 409PC instrument was used to analyze the thermal stability. Crystalline samples of RWOFI and CWOFI were placed in a crucible and heated from 30 to 700 °C at a rate of $10 \text{ }^\circ\text{C}\cdot\text{min}^{-1}$ under a nitrogen atmosphere with an empty crucible used as a reference.

3.5 Second-Harmonic Generation

The SHG effects of RWOFI and CWOFI were investigated with sieved samples by employing the adapted method of Kurtz and Perry.^[3] A Q-switched Nd:YAG laser with 1064 nm radiation was employed for measurement. Since the powder SHG efficiency is related to the particle size, the crystalline samples were ground and sieved into different particle size ranges (<26, 26–50, 50–74, 74–105, 105–150, 150–200, and 200–280 μm), which were pressed into disks of diameter 6 mm that were placed between glass microscope slides and secured with tape in a 1 mm thick aluminum holder. Crystalline KH_2PO_4 (KDP) was dealt with in the same way and used as a reference.

4. Theoretical Calculations

First-principles calculations were carried out using the CASTEP package on energetically stable optimized structures of RWOFI and CWOFI to obtain optical and electronic properties results.^[4] A plane-wave basis set and pseudopotential density functional theory (DFT) were utilized.^[5,6] The generalized gradient approximation^[8] scheme of Perdew-Burke-Ernzerhof^[7] was employed to describe the exchange-correlation interaction. The cut-off value of the kinetic energy is 400 eV with condensed Monkhorst-Pack^[10] k-point grid spanning below 0.2 \AA^{-3} in the Brillouin zone, which ensured the accuracy of the calculations. Owing to the discontinuity of the exchange–correlation of standard DFT, the calculated bandgaps are narrower compared to the experimental results, so a scissor operator was adopted to shift the conduction band to match the measured value.^[11] Based on the scissor-corrected electronic structure, the imaginary part of the dielectric function can be calculated by the electronic transition from the forbidden band, and the real part, such as the refractive index, can be obtained using the Kramers-Kronig transformation.^[12] The anisotropic NLO tensors were further computed according to the formula developed by our group.^[13,14] To ascertain the contributing percentages of the component groups, the real-space atom-cutting analysis and the SHG-weighted electronic density were calculated.^[15,16]

Table S1. Crystallographic data and structure refinement parameters for RWOFI and CWOFI.

| formula | Rb ₂ WO ₂ F ₃ (IO ₂ F ₂) | Cs ₂ WO ₂ F ₃ (IO ₂ F ₂) |
|--|--|--|
| formula weight | 640.69 | 735.57 |
| temperature (K) | 296(2) K | 294(2) K |
| crystal system | Orthorhombic | Orthorhombic |
| space group | <i>Cmc2</i> ₁ | <i>Cmc2</i> ₁ |
| <i>a</i> (Å) | 11.726(2) | 12.1122(6) |
| <i>b</i> (Å) | 10.188(2) | 10.6192(6) |
| <i>c</i> (Å) | 7.6661(16) | 7.8333(4) |
| α (°) | 90 | 90 |
| β (°) | 90 | 90 |
| γ (°) | 90 | 90 |
| <i>V</i> (Å ³) | 915.8(3) | 1007.53(9) |
| <i>Z</i> | 4 | 4 |
| ρ_{calc} (g cm ⁻³) | 4.647 | 4.849 |
| μ (mm ⁻¹) | 26.607 | 21.707 |
| <i>F</i> (000) | 1112 | 1256 |
| θ (deg.) | 2.648–24.978 | 2.551–27.083 |
| limiting indices | $-13 \leq h \leq 13$, $-12 \leq k \leq 12$, $-9 \leq l \leq 9$ | $-15 \leq h \leq 15$, $-13 \leq k \leq 10$, $-9 \leq l \leq 10$ |
| <i>R</i> _{int} | 0.0563 | 0.0342 |
| no. of reflections (collected/unique) | 3604/821 | 2933/1111 |
| absolute structure parameter | 0.32(10) | 0.02(2) |
| goodness of fit on <i>F</i> ² | 1.020 | 1.083 |
| <i>R</i> ₁ , <i>wR</i> ₂ [<i>I</i> > 2σ(<i>I</i>)] ^[a] | 0.0773/0.1834 | 0.0279/0.0599 |
| <i>R</i> ₁ , <i>wR</i> ₂ (all data) | 0.0774/0.1834 | 0.0291/0.0604 |
| largest difference peak and hole (e Å ⁻³) | 4.248 and -5.754 | 1.367 and -1.188 |

^a $R_1 = \sum ||F_o| - |F_c|| / \sum |F_o|$; $wR_2 = [\sum w(F_o^2 - F_c^2)^2] / [\sum w(F_o^2)]^{1/2}$

Table S2. Selected bond distances (\AA) and angles (deg) for RWOI.

| | | | |
|-------------------|----------|--------------------|-----------|
| I(1A)-O(1) | 1.73(9) | F(1)-Rb(1) | 2.96(6) |
| I(1A)-O(2) | 1.84(5) | F(1)-Rb(1)#8 | 3.14(6) |
| I(1A)-F(1) | 1.93(4) | F(1)-Rb(1)#5 | 3.59(5) |
| I(1A)-F(1)#1 | 1.93(4) | F(2)-Rb(1)#9 | 2.80(4) |
| I(1B)-F(1)#1 | 1.57(7) | F(2)-Rb(1) | 2.87(4) |
| I(1B)-O(2) | 2.07(8) | O(3)-Rb(1)#5 | 2.85(5) |
| I(1B)-O(1) | 2.38(11) | O(3)-Rb(1) | 3.07(5) |
| W(1)-F(3) | 1.67(8) | O(3)-Rb(1)#3 | 3.58(5) |
| W(1)-O(3)#1 | 1.80(5) | O(1)-Rb(1)#4 | 3.05(6) |
| W(1)-O(3) | 1.80(5) | O(1)-Rb(1)#5 | 3.05(6) |
| W(1)-F(2) | 1.97(4) | F(3)-Rb(1)#2 | 2.91(5) |
| W(1)-F(2)#1 | 1.97(4) | F(3)-Rb(1)#3 | 2.91(5) |
| W(1)-O(2) | 2.25(5) | F(3)-W(1)-O(3) | 101(2) |
| O(1)-I(1A)-O(2) | 101(3) | O(3)#1-W(1)-O(3) | 101(3) |
| O(1)-I(1A)-F(1) | 88.0(17) | F(3)-W(1)-F(2) | 99(2) |
| O(2)-I(1A)-F(1) | 89(2) | O(3)#1-W(1)-F(2) | 157.6(18) |
| O(1)-I(1A)-F(1)#1 | 88.0(17) | O(3)-W(1)-F(2) | 86.1(17) |
| O(2)-I(1A)-F(1)#1 | 89(2) | F(3)-W(1)-F(2)#1 | 99(2) |
| F(1)-I(1A)-F(1)#1 | 175(3) | O(3)#1-W(1)-F(2)#1 | 86.1(17) |
| F(1)#1-I(1B)-O(2) | 92(4) | O(3)-W(1)-F(2)#1 | 157.6(18) |
| F(1)#1-I(1B)-O(1) | 77(3) | F(2)-W(1)-F(2)#1 | 80(2) |
| O(2)-I(1B)-O(1) | 76(3) | F(3)-W(1)-O(2) | 175(3) |
| F(2)-W(1)-O(2) | 77.9(15) | O(3)#1-W(1)-O(2) | 81.9(16) |
| F(2)#1-W(1)-O(2) | 77.9(15) | O(3)-W(1)-O(2) | 81.9(16) |
| F(3)-W(1)-O(3)#1 | 101(2) | | |

Symmetry codes: #1 -x, y, z; #2 x-1/2, y-1/2, z; #3 -x+1/2, y-1/2, z; #4 x-1/2, -y+1/2, z-1/2; #5 -x+1/2, -y+1/2, z-1/2; #6 -x, -y+1, z-1/2; #7 x-1/2, y+1/2, z; #8 x, -y+1, z-1/2; #9 -x+1/2, -y+1/2, z+1/2; #10 x+1/2, y+1/2, z; #11 x, -y+1, z+1/2; #12 -x+1/2, y+1/2, z; #13 -x, -y+1, z+1/2; #14 x+1/2, y-1/2, z

Table S3. Selected bond distances (\AA) and angles (deg) for CWOFI.

| | | | |
|--------------------|-----------|------------------|-----------|
| I(1)-O(1) | 1.759(14) | O(1)-Cs(1)#6 | 3.176(10) |
| I(1)-O(2) | 1.790(17) | O(1)-Cs(1)#7 | 3.176(10) |
| I(1)-F(1) | 1.974(8) | F(1)-Cs(1) | 3.055(9) |
| I(1)-F(1)#1 | 1.974(8) | F(1)-Cs(1)#8 | 3.203(9) |
| W(1)-F(3) | 1.733(16) | F(2)-Cs(1)#5 | 3.006(8) |
| W(1)-O(3) | 1.800(10) | F(2)-Cs(1) | 3.026(8) |
| W(1)-O(3)#1 | 1.800(10) | O(3)-Cs(1)#7 | 3.077(10) |
| W(1)-F(2) | 1.953(8) | O(3)-Cs(1) | 3.365(10) |
| W(1)-O(2) | 2.263(17) | O(3)-Cs(1)#3 | 3.463(10) |
| W(1)-F(2)#1 | 1.953(8) | F(3)-Cs(1)#2 | 3.137(11) |
| O(1)-I(1)-O(2) | 105.2(7) | O(3)-W(1)-F(2)#1 | 161.8(4) |
| O(1)-I(1)-F(1)#1 | 89.4(3) | F(3)-W(1)-F(2) | 96.7(5) |
| O(2)-I(1)-F(1)#1 | 89.3(3) | O(3)#1-W(1)-F(2) | 161.8(4) |
| O(1)-I(1)-F(1) | 89.4(3) | O(3)-W(1)-F(2) | 88.1(4) |
| O(2)-I(1)-F(1) | 89.3(3) | F(2)#1-W(1)-F(2) | 80.9(5) |
| F(1)#1-I(1)-F(1) | 177.8(6) | F(3)-W(1)-O(2) | 172.6(7) |
| F(3)-W(1)-O(3)#1 | 99.0(5) | O(3)#1-W(1)-O(2) | 85.8(4) |
| F(3)-W(1)-O(3) | 99.0(5) | O(3)-W(1)-O(2) | 85.8(4) |
| O(3)#1-W(1)-O(3) | 98.5(6) | F(2)#1-W(1)-O(2) | 77.8(4) |
| F(3)-W(1)-F(2)#1 | 96.7(5) | F(2)-W(1)-O(2) | 77.8(4) |
| O(3)#1-W(1)-F(2)#1 | 88.1(4) | | |

Symmetry codes: #1 -x, y, z; #2 x-1/2, y-1/2, z; #3 -x+1/2, y-1/2, z; #4 x-1/2, -y+1/2, z-1/2; #5 -x+1/2, -y+1/2, z-1/2; #6 -x, -y+1, z-1/2; #7 x-1/2, y+1/2, z; #8 x, -y+1, z-1/2; #9 -x+1/2, -y+1/2, z+1/2; #10 x+1/2, y+1/2, z; #11 x, -y+1, z+1/2; #12 -x+1/2, y+1/2, z; #13 -x, -y+1, z+1/2; #14 x+1/2, y-1/2, z

Table S4. Atomic coordinates, equivalent isotropic displacement parameters, and bond valence sums for each atom in the asymmetric unit of RWOFI.

| Atom | <i>x</i> | <i>y</i> | <i>z</i> | U _{eq} (Å ²) | BVS |
|-------|----------|----------|-----------|-----------------------------------|------|
| W(1) | 0 | 1616(3) | 4355(2) | 26(1) | 6.24 |
| I(1A) | 0 | 4766(5) | 1638(7) | 14(1) | 5.21 |
| I(1B) | -440(50) | 5300(70) | 2010(80) | 14(1) | 3.26 |
| F(1) | 1650(40) | 4680(50) | 1630(90) | 76(13) | 1 |
| F(2) | 1080(30) | 2360(40) | 6050(50) | 45(9) | 0.98 |
| F(3) | 0 | 60(80) | 5060(100) | 78(19) | 1.75 |
| O(1) | 0 | 3550(90) | 60(100) | 70(20) | 2.12 |
| O(2) | 0 | 3760(50) | 3640(70) | 21(11) | 1.97 |
| O(3) | 1180(40) | 1590(40) | 2860(60) | 43(11) | 1.72 |
| Rb(1) | 3061(4) | 3368(7) | 4323(11) | 42(2) | 1.1 |

Table S5. Atomic coordinates, equivalent isotropic displacement parameters, and bond valence sums for each atom in the asymmetric unit of CWOFI.

| Atom | <i>x</i> | <i>y</i> | <i>z</i> | U _{eq} (Å ²) | BVS |
|-------|----------|-----------|-----------|-----------------------------------|------|
| W(1) | 5000 | 11808(1) | 6435(1) | 20(1) | 5.76 |
| I(1) | 5000 | 14674(1) | 9399(1) | 17(1) | 5.1 |
| O(1) | 5000 | 13526(14) | 11018(18) | 27(3) | 2.19 |
| O(2) | 5000 | 13806(16) | 7440(20) | 37(4) | 2.18 |
| O(3) | 6126(8) | 11543(10) | 7891(12) | 24(2) | 1.71 |
| F(1) | 6630(7) | 14638(10) | 9390(12) | 41(2) | 0.93 |
| F(2) | 6046(6) | 12641(9) | 4910(10) | 29(2) | 0.99 |
| F(3) | 5000 | 10363(15) | 5406(19) | 50(4) | 1.42 |
| Cs(1) | 8137(1) | 13528(1) | 6650(1) | 29(1) | 0.95 |

Table S6. Calculated magnitudes and directions of dipole moments of RWOFI and CWOFI.

| Crystal | building units | Dipole moment | | | | $\times 10^{-22}$ esu cm Å $^{-3}$ |
|--|---|---------------|------|-------|------|------------------------------------|
| | | x(a) | y(b) | z(c) | net | |
| Rb ₂ WO ₂ F ₃ (IO ₂ F ₂) | [WO ₃ F ₃] ³⁻ | 0 | 0 | -5.2 | 5.2 | 56.8 |
| | [IO ₂ F ₂] ⁻ | 0 | 0 | 7.56 | 7.56 | 82.6 |
| | Unit cell | 0 | 0 | 2.36 | 2.36 | 25.8 |
| Cs ₂ WO ₂ F ₃ (IO ₂ F ₂) | [WO ₃ F ₃] ³⁻ | 0 | 0 | -6.04 | 6.04 | 60 |
| | [IO ₂ F ₂] ⁻ | 0 | 0 | 8.25 | 8.25 | 81.9 |
| | Unit cell | 0 | 0 | 2.21 | 2.21 | 21.9 |

Table S7. Contributions of different units to the SHG response and birefringence of RWOFI and CWOFI.

| | Total | $[\text{IO}_2\text{F}_2]^-$ | $[\text{WO}_3\text{F}_3]^{3-}$ | $[\text{WO}_2\text{F}_3\text{IO}_2\text{F}_2]^{2-}$ | Rb^+/Cs^+ |
|--|------------|-----------------------------|--------------------------------|---|---------------------------|
| n_x | 1.615 | 1.579 | 1.389 | 1.689 | 1.386 |
| n_y | 1.449 | 1.381 | 1.352 | 1.473 | 1.383 |
| n_z | 1.449 | 1.465 | 1.367 | 1.619 | 1.38 |
| Rb ₂ WO ₂ F ₃ (IO ₂ F ₂) | Δn | 0.166 | 0.198 | 0.037 | 0.03 |
| | d_{32} | 0.62 | 0.89 | 0.36 | 1.12 |
| | d_{31} | 1.59 | 1.98 | 0.77 | 1.23 |
| | d_{33} | 0.15 | 0.23 | 0.03 | 0.11 |
| | n_x | 1.774 | 1.532 | 1.359 | 1.658 |
| | n_y | 1.637 | 1.376 | 1.303 | 1.496 |
| | n_z | 1.771 | 1.493 | 1.376 | 1.598 |
| Cs ₂ WO ₂ F ₃ (IO ₂ F ₂) | Δn | 0.137 | 0.156 | 0.056 | 0.011 |
| | d_{32} | 1.41 | 1.32 | 0.98 | 1.65 |
| | d_{31} | 1.85 | 1.67 | 0.68 | 1.43 |
| | d_{33} | 0.19 | 0.09 | 0.05 | 0.06 |
| | | | | | 0.09 |

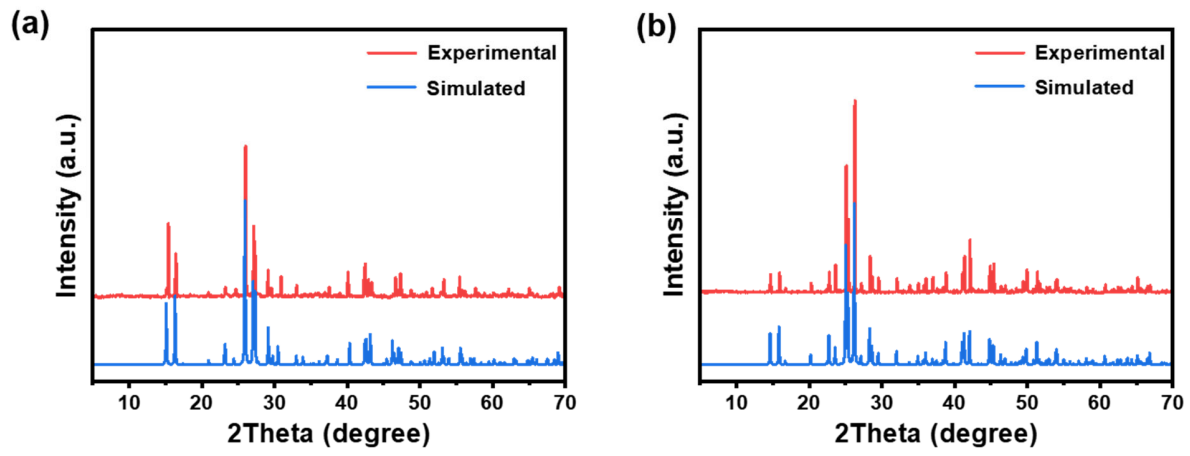


Figure S1. Experimental and simulated powder X-ray diffraction patterns of RWOFI (a) and CWOFI (b).

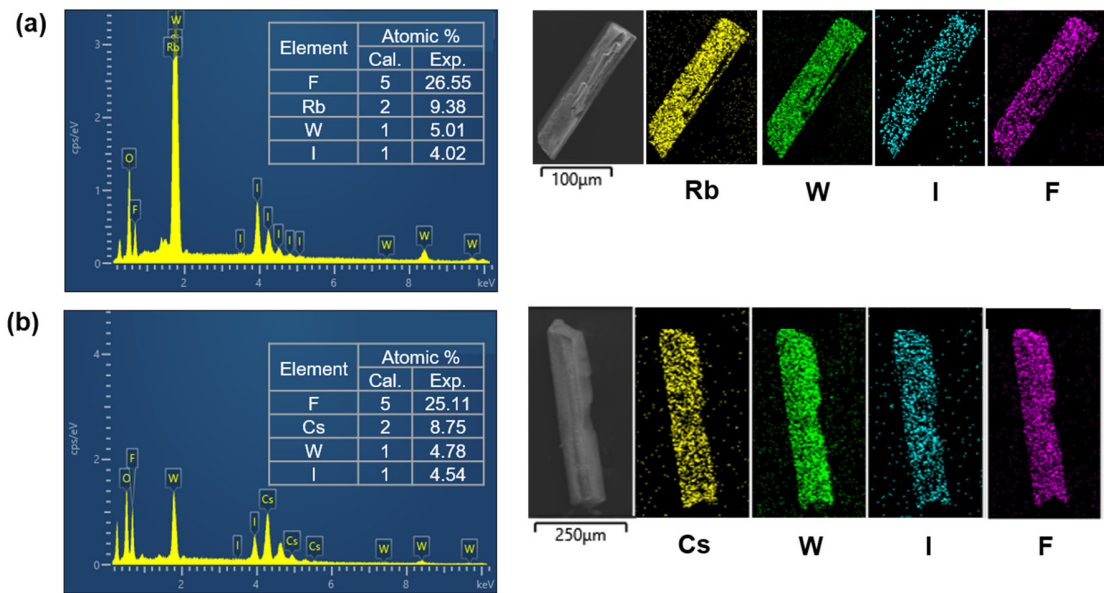


Figure S2. Scanning electron microscope images and energy dispersive spectroscopy results of RWOFI (a) and CWOFI (b).

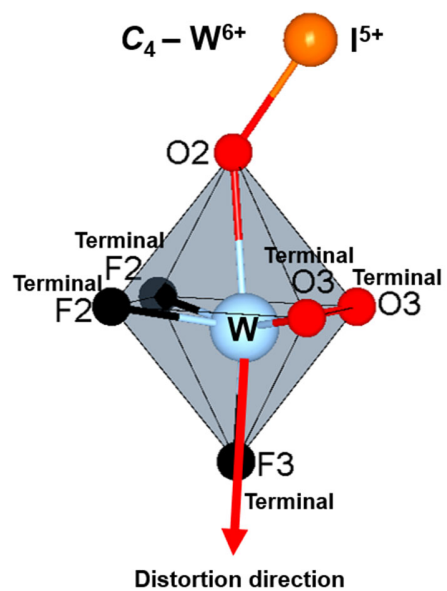


Figure S3. Out-of-center distortion for W^{6+} in CWOFI; the distortion is away from the oxide ligands that link to a lone-pair cation.

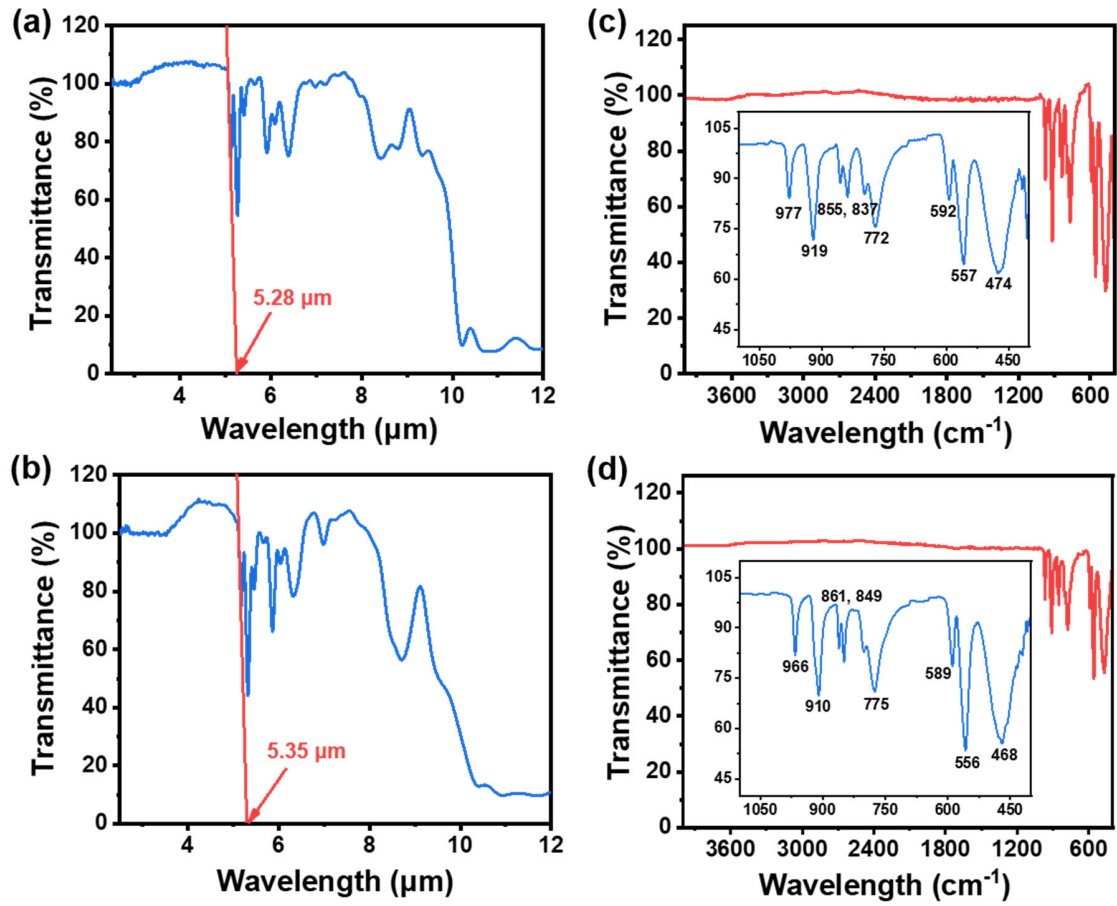


Figure S4. IR transmission spectra from single crystals (a, b) and crystalline powder samples (c, d) of RWOFI and CWOFI. The inserts show the detailed IR absorption peaks.

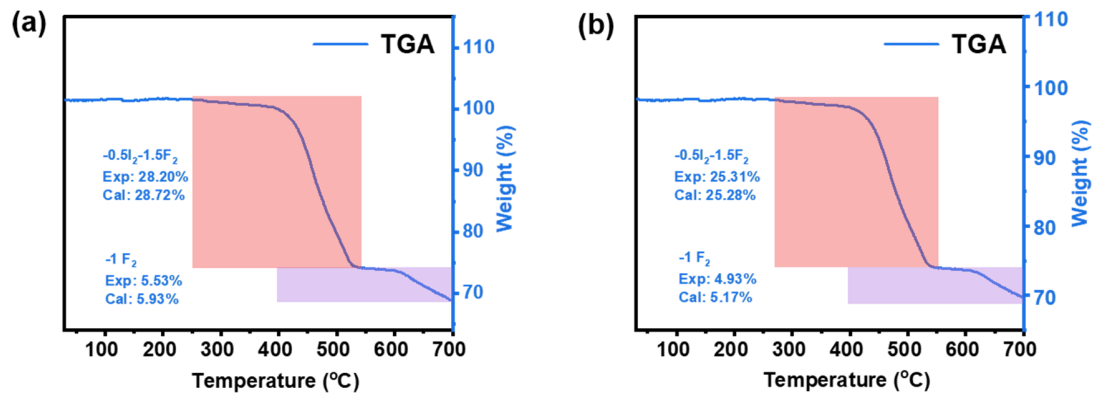


Figure S5. Thermogravimetric analyses of RWOI (a) and CWOI (b) under a N₂ atmosphere.

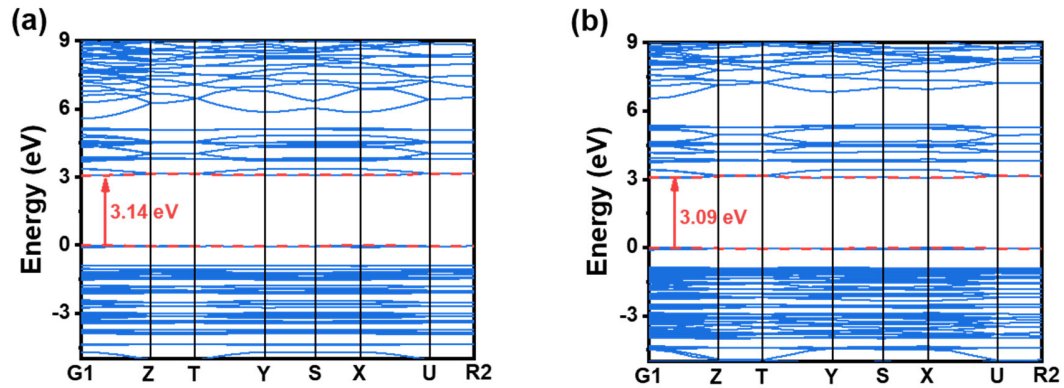


Figure S6. Calculated band structures of RWOFI (a) and CWOFI (b).

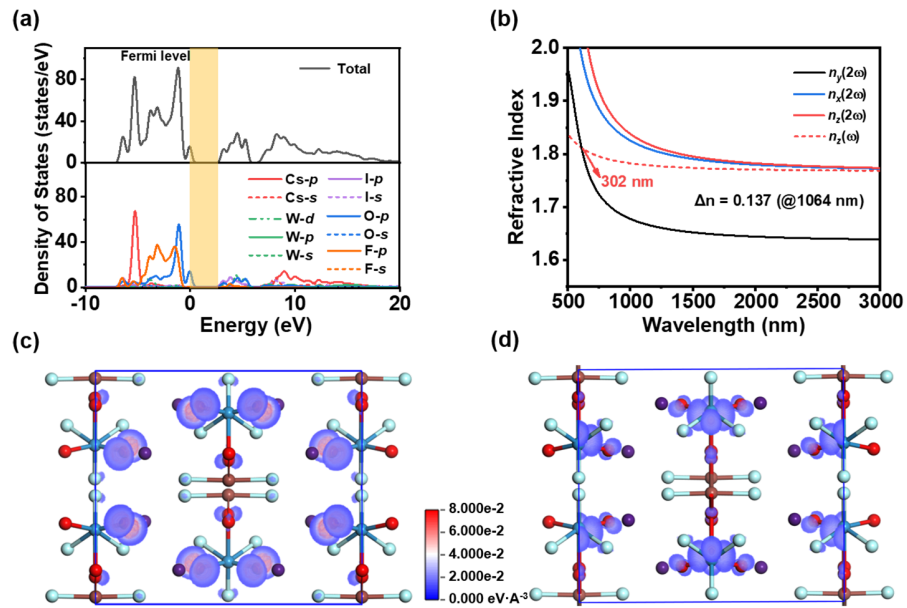


Figure S7. Calculated density of states (a) and refractive indexes (b) in CWOFI. SHG-weighted densities for (c) occupied and (d) unoccupied states in the virtual electron process for CWOFI. Color codes: I brown, Mo green, O red, F light green, Cs purple.

References

- [1] G. M. Sheldrick, *Acta Crystallogr. Sect. C: Struct. Chem.* **2015**, *C71*, 3-8.
- [2] A. L. Spek, *J. Appl. Crystallogr.* **2003**, *36*, 7-13.
- [3] S. K. Kurtz, T. T. Perry, *J. Appl. Phys.* **1968**, *39*, 3798-3813.
- [4] S. J. Clark, M. D. Segall, C. J. Pickard, P. J. Hasnip, M. I. J. Probert, K. Refson, M. C. Payne, *Z. Kristallogr.* **2005**, *220*, 567-570.
- [5] W. Kohn, L. J. Sham, *Phys. Rev.* **1965**, *140*, 1133-1138.
- [6] M. C. Payne, M. P. Teter, D. C. Allan, T. A. Arias, J. D. Joannopoulos, *Rev. Mod. Phys.* **1992**, *64*, 1045-1097.
- [7] J. P. Perdew, K. Burke, M. Ernzerhof, *Phys. Rev. Lett.* **1996**, *77*, 3865-3868.
- [8] J. P. Perdew, Y. Wang, *Phys. Rev. B: Condens. Matter Mater. Phys.* **1992**, *46*, 12947-12954.
- [9] D. R. Hamann, M. Schluter, C. Chiang, *Phys. Rev. Lett.* **1979**, *43*, 1494-1497.
- [10] H. J. Monkhorst, J. D. Pack, *Phys. Rev. B: Solid State* **1976**, *13*, 5188-5192.
- [11] R. W. Godby, M. Schluter, L. J. Sham, *Phys. Rev. B: Condens. Matter Mater. Phys.* **1988**, *37*, 10159-10175.
- [12] E. D. Palik, *Handbook of Optical Constants of Solids*; Academic: New York, **1985**.
- [13] Z. S. Lin, X. X. Jiang, L. Kang, P. F. Gong, S. Y. Luo, M. H. Lee, *J. Phys. D: Appl. Phys.* **2014**, *47*, 253001.
- [14] J. Lin, M. H. Lee, Z. P. Liu, C. T. Chen, C. J. Pickard, *Phys. Rev. B: Condens. Matter Mater. Phys.* **1999**, *60*, 13380-13389.
- [15] R. He, Z. S. Lin, M. H. Lee, C. T. Chen, *J. Appl. Phys.* **2011**, *109*, 103510.
- [16] M. H. Lee, C. H. Yang, J. H. Jan, *Phys. Rev. B: Condens. Matter Mater. Phys.* **2004**, *70*, 235110.